acta physica slovaca vol. 47 No. 3/4, 179 – 184 June 1997

QUANTUM AND CLASSICAL DESCRIPTION OF THREE-WAVE INTERACTION[1]

A. Bandilla[2]
Humboldt–Universität zu Berlin, Institut für Physik,
Rudower Chaussee 5, 12484 Berlin, Germany

G. Drobný
Institute of Physics, Slovak Academy of Sciences, Dúbravská cesta 9,
842 28 Bratislava, Slovakia

I. Jex
Department of Physics, FJFI ČVUT,
Břehová 7, 115 19 Praha 1 - Staré Město, Czech Republic

Received 5 May 1997, accepted 12 May 1997

The classical and quantum mechanical description of three-wave interaction are summarized and compared. There is a far-reaching equivalence but characteristic differences exist. Exact quantum mechanical results via numerical solutions were already found for medium initial photon numbers. The calculation of the Wigner function with the help of classical trajectories offers a very good approximation for the quantum mechanical description in region of arbitrarily large mean photon numbers. In addition, the trajectories help us to understand the processes physically.

Parametric interaction between intense light beams is the most important process for the generation of squeezed states [1] and is by now classically well understood [2,3]. Its optical history began with the observation of the second harmonic of a laser [4] and was shortly after this followed by exact solutions for the classical coupled-mode equations of three- and four-wave interactions [5]. Although these solutions describe most of the experiments they do not allow immediately to extract the behavior of the single phases [6]. The normally much more important phase difference can be inferred from the conserved quantity Γ [5].

To be more definite let us confine ourselves to $\chi^{(2)}$ media and consider only three-wave interaction including the degenerate case of second-harmonic generation (SHG).

[1] Presented at the **Fifth Central-European Workshop on Quantum Optics**, Prague, Czech Republic, April 25 - 28, 1997

[2] E-mail address: bandilla@photon.fta-berlin.de

0323-0465/97

The application to other nonlinearities is discussed in [7]. For exact resonance we have $\omega_3 = \omega_1 + \omega_2$, where ω_3 is the frequency of the pump and ω_1 and ω_2 correspond to signal and idler, respectively. We assume throughout this paper phase matching of the wave vectors. The above mentioned Γ takes then the form [5]

$$\Gamma = u_1(\zeta)u_2(\zeta)u_3(\zeta)\cos\theta(\zeta), \tag{1}$$

where $u_i(\zeta)$, $(i = 1,2,3)$ are the real classical amplitudes and $\theta = \varphi_3 - \varphi_2 - \varphi_1$ their phase difference.

The corresponding quantum problem of three-wave interaction is described by the Hamiltonian (in the interaction picture)

$$\hat{H}_{int} = \hbar\kappa(\hat{a}\hat{b}\hat{c}^\dagger + \hat{a}^\dagger\hat{b}^\dagger\hat{c}), \tag{2}$$

where $\hat{a}, \hat{b}$ and $\hat{c}$ are the annihilation operators of signal, idler and pump, respectively, and κ is the coupling constant containing $\chi^{(2)}$. The classical constant Γ corresponds to the expectation value of the Hamiltonian (2) for coherent states.

To complete the classical picture we consider the squared pump amplitude $u_3^2(\zeta)$ as given by [5]

$$u_3^2(\zeta) = u_{3a}^2 + (u_{3b}^2 - u_{3a}^2)\,\mathrm{sn}^2[(u_{3c}^2 - u_{3a}^2)^{1/2}(\zeta + \zeta_0), m], \tag{3}$$

where $\mathrm{sn}[x, m]$ is the Jacobian elliptic function [8] and the parameter m is given by

$$m = \frac{u_{3b}^2 - u_{3a}^2}{u_{3c}^2 - u_{3a}^2}. \tag{4}$$

The constants $u_{3c}^2 \geq u_{3b}^2 \geq u_{3a}^2$ are the roots of the equation

$$u_3^2[u_1^2(0) + u_3^2(0) - u_3^2][u_2^2(0) + u_3^2(0) - u_3^2] - \Gamma^2 = 0. \tag{5}$$

The coordinate $\zeta = \kappa t$ is proportional to the interaction length and contains the coupling constant κ from (2). The solution (3) depends only via Γ on the phase difference. The intensities of signal and idler can then be written as $u_i^2(\zeta) = u_i^2(0) + u_3^2(0) - u_3^2(\zeta)$, $i = 1,2$. Finally, the single phases behave according to [2,9]

$$\varphi_i(\zeta) = \varphi_i(0) - \int_0^\zeta \frac{\Gamma}{u_1^2(\zeta')}d\zeta', \quad i = 1,2,3, \tag{6}$$

where $\Gamma \neq 0$ secures that also $u_i^2(\zeta)$ cannot become zero.

We mention that this classical picture is greatly simplified in the parametric approximation where the pump is very strong and does not feel any depletion. Then we can express the complex signal and idler amplitudes by

$$\alpha(\zeta) = \alpha\cosh(u_3(0)\zeta) - ie^{-i\varphi_3}\beta^*\sinh(u_3(0)\zeta)$$

$$\beta(\zeta) = \beta\cosh(u_3(0)\zeta) - ie^{-i\varphi_3}\alpha^*\sinh(u_3(0)\zeta). \tag{7}$$

In (7) $\alpha(\beta)$ is the initial complex amplitude of the signal (idler) wave and the phase motions are automatically included. If, for instance, all modes start real then they become immediately complex and show so phase changes. The no-energy exchange regime [2,6] is impossible and we emphasize that the exact classical solution for a strong pump shows that almost all pump energy can be transferred irrespective of the initial phase difference. This is very different from a situation where all three initial intensities are comparable.

The exact quantum mechanical solutions can only be obtained numerically, e.g., via diagonalization in the number-state basis [10]. Such quantum mechanical calculations (with all modes excited initially, as, e.g., in [6]) are naturally limited to relatively small average photon numbers but include all saturation phenomena which correspond to the classical nonlinearities describing depletion. The question arises if we can use the various classical motions to get a deeper understanding of the quantum motion and simultaneously extend the quantum calculations to arbitrary high photon numbers. It turns out that by using ensembles of classical trajectories that fit to the initial Wigner distributions W we can describe quantum mechanically almost all nonlinear optical effects for a time region that extends at least up to the first depletion of one mode. Note that within this time region the most important quantum effects as squeezing and sub-Poissonian statistics reach their (first) maximum. The limits show up as significant negativities in the exact W [7]. On the other hand this method includes negative W functions from the beginning.

Therefore we make the following ansatz for the Wigner function of all three modes

$$W(\alpha,\beta,\gamma;t) \approx W(\alpha_{0c}(\alpha,\beta,\gamma,t), \beta_{0c}(\alpha,\beta,\gamma,t), \gamma_{0c}(\alpha,\beta,\gamma,t); 0), \tag{8}$$

where $\wp(t) = \{\alpha_{0c}, \beta_{0c}, \gamma_{0c}\}$ is a classical trajectory which at time t reaches the phase-space point $\{\alpha,\beta,\gamma\}$. The classical trajectories, i.e., solutions of the classical equations of motion, are inserted on r.h.s. in the initial W distribution of the modes. In other words, the quantum dynamics in phase space [given by Eq.(8)] is simulated within the classical phase space starting with an ensemble of phase-space points according to the initial Wigner distributions. Monte Carlo methods of importance sampling can be applied to calculate quantities of interest.

The accuracy of such an approach can be estimated. When we look at the exact equation for W we see that it has no second-order derivatives but there are third-order derivatives which will be neglected by our method using classical trajectories. On the other hand, by assuming coherent states initially in all modes, i.e., $|\psi(0)\rangle = |\alpha_0\rangle_a|\beta_0\rangle_b|\gamma_0\rangle_c$, we can expand the Wigner function up to second order in (κt) and compare this with corresponding expansions inserting classical trajectories. These calculations show that the error can be surprisingly small if we consider only one mode and average over the others. For example, the exact Wigner function of the signal is given up to second order in (κt) by

$$\begin{aligned} W_a(\alpha,t) = 2e^{-2|\alpha-\alpha_0|^2}\,[1 &- \{i\kappa t 2(\alpha^* - \alpha_0^*)\beta_0^*\gamma_0^* + c.c.\} \\ &+(\kappa t)^2\left(\{-2(\alpha^* - \alpha_0^*)^2\beta_0^{*2}\gamma_0^2 + c.c.\} + 2|\alpha - \alpha_0|^2(2|\beta_0|^2|\gamma_0|^2 + |\beta_0|^2 + |\gamma_0|^2)\right. \\ &\left.+(|\gamma_0|^2 - |\beta_0|^2)\{\alpha(\alpha^* - \alpha_0^*) + c.c.\} - 2|\gamma_0|^2(|\beta_0|^2 + 1)) + O((\kappa t)^3)\right]. \end{aligned} \tag{9}$$

If we use a short-time expansion for the classical amplitudes and insert them as trajectories into the Gaussians of the initial W we find also (9) except that in second order the term $|\alpha - \alpha_0|^2 - 1/2$ has to be added.

For a variety of initial conditions numerical simulations were compared with exact quantum results for medium initial photon numbers. The tendency that the agreement improves with increasing initial photon numbers was demonstrated for different examples in [7]. So we could go over to very large photon numbers and derive scaling laws [7].

Here, we concentrate on the initial state

$$|\psi(0)\rangle = |\alpha_0 = 8\rangle_a|0\rangle_b|\gamma_0 = 80\rangle_c \tag{10}$$

which describes for $\gamma \to \infty$ and relative small α the linear phase-insensitive parametric amplifier. Such an amplifier is completely equivalent to a linear laser amplifier where all active atoms start in the excited level [11]. The new point here is that we consider also the nonlinear behaviour of the signal amplification in (10) up to the almost complete exhaustion of the pump and try to understand all this with the help of characteristic classical trajectories.

Eq. (5) has three real roots because for $\Gamma = 0$ [$\cos\theta(0) = 0$ or one $u_i(0) = 0$] the roots are

$$u_{3a}^2 = 0, \quad u_{3b}^2 = u_1^2(0) + u_3^2(0), \quad u_{3c}^2 = u_2^2(0) + u_3^2(0) \qquad (u_1^2(0) \geq u_2^2(0)). \tag{11}$$

Furthermore, for the largest $\Gamma^2 = u_1^2(0)u_2^2(0)u_3^2(0)$ one root is given exactly by $u_3^2(0)$ and the other two are found from a quadratic equation with real roots. All other cases are in between what makes the above statement about the roots plausible. These three roots determine the "range of power variation" [5].

For the initial state (10) and allowing a spectrum of classical initial amplitudes according to Wigner functions for these coherent states, the parameter m given in (4) turns out to almost constant and very close to 1. We note that u_{3a}^2 determines in (3) the smallest pump amplitude. Small values of Γ are typical for all pump amplitudes lying within the initial distributions of the Wigner function and imply also u_{3a}^2 close to zero [see Eq.(11)]. Therefore it comes to a constriction of the pump Wigner function when the (quantum mechanical) pump amplitude passes zero. This is shown in Fig. 1.

In addition the distribution is strongly stretched what can also be understood by inspecting (3): For $m \to 1$ the elliptic sn function can be approximated by the hyperbolic tangent. The constant ζ_0 has to be chosen in such a way that the argument becomes zero when the pump reaches its minimum. Near to this zero the function tanh varies most strongly. Therefore the relatively weak variation of ζ_0 due to different initial values in signal and idler has a large effect on the pump amplitudes when the last are already relatively small.

When the pump starts being depleted the single values of $u_3^2(\zeta)$ are very strong. Consequently their phases are almost constant according to (6) and so the pump points move radially. This leads to pump phase squeezing what is also clear from Fig. 1. Simultaneously the amplitude and photon number fluctuations increase.

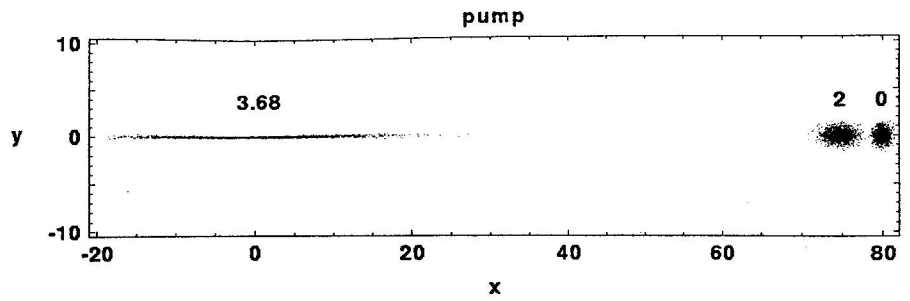

Fig. 1. Density sampling of the simulated Wigner function of the pump wave at times $\gamma\zeta = 0, 2,$ and 3.68 when the amplitude $\langle\psi|\hat{c}|\psi\rangle$ passes zero.

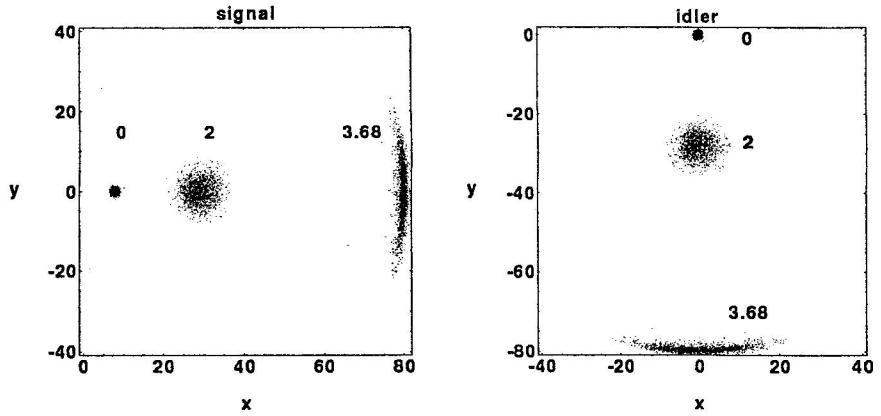

Fig. 2. Simulated Wigner function of the signal and idler wave at same times as in Fig. 1. At the time $\gamma\zeta = 2$ the signal looks still as linearly amplified [see Eq.(7)] although Fig. 1 shows already a clear deformation of the pump.

The change of the Wigner function for signal and idler is depicted in Fig. 2. Initially the pump is almost constant while the signal and especially the idler phases adjust quickly to optimum phase values so that the energy transfer becomes maximum (compare [2]). This leads to an enlargement of the signal phase uncertainty well-known from linear amplification [11,12]. The signal cloud blows up but moves simultaneously to greater amplitude values as shown in Fig. 2. This behaviour is understandable by using the solutions (7). For an arbitrary pair of initial values for signal and idler these solutions have an exponentially growing part and one which is damped out. The growing part shows that the asymptotic angle of each signal point with the positive real axis is equal to the angle that the corresponding idler constitutes with the negative imaginary

axis. Therefore, the broadening of the phase in both waves is equal. In the saturation regime these angles cannot change due to (6). Concerning the amplifier it is well-known that the quantum phase distribution of a greatly amplified signal becomes stationary [11]. This can here traced back to single trajectories.

When the pump cloud crosses zero, signal and idler come into complete saturation and show a crescent-like distribution of almost constant amplitudes and a phase distribution that corresponds to the broadened one of the initial signal. But there is no phase saturation. These results can be compared with the description of a saturated laser amplifier [13,14]. The saturated laser amplifier leads to amplitude stabilization but does not limit the phase diffusion.

Note that there is a remaining pump photon number that cannot be depleted. For an initial signal ($\alpha = 2$) approximately 10% of the initial pump photon number stay there. Calculations with greater pump amplitudes ($\gamma = 40$, 160, 640) and the same signal give similar results. This fraction is reduced with increase of the coherent signal input and goes to zero when all three waves have comparable strengths and a phase difference $\theta(0) = \pi/2$.

References

[1] Special issue on squeezed states of the electromagnetic field, ed. by H.J. Kimble, D.F. Walls: *J. Opt. Soc. Am. B* **4** (1987) 1450; special issue on squeezed states, ed. by R. Loudon, P.L. Knight: *J. Mod. Opt.* **34** (1987) 709

[2] A. Bandilla, G. Drobný, I. Jex: *Opt. Commun.* **128** (1996) 353

[3] A. Kobyakov, U. Peschel, F. Lederer: *Opt. Commun.* **124** (1995) 184

[4] P. Franken, A.E. Hill, C.W. Peters, G. Weinreich: *Phys. Rev. Lett.* **7** (1961) 118

[5] J.A. Armstrong, N. Bloembergen, J. Ducuing, P.S. Pershan: *Phys. Rev.* **127** (1962) 1918

[6] A. Bandilla, G. Drobný, I. Jex: *Phys. Rev. Lett.* **75** (1995) 4019; *Phys. Rev. A* **53** (1996) 507

[7] G. Drobný, A. Bandilla, I. Jex: *Phys. Rev. A* **55** (1997) 78

[8] M. Abramowitz, I.A. Stegun: *Handbook of Mathematical Functions* (New York, Dover, 1972)

[9] A. Bandilla, G. Drobný, I. Jex: *Acta Physica Slovaca* **46** (1996) 221

[10] D.F. Walls, R. Barakat: *Phys. Rev. A* **1** (1970) 446

[11] A. Bandilla, H. Paul: *Ann. Physik* **23** (1969) 323; A. Bandilla, H. Paul: *Ann. Physik* **24** (1970) 119

[12] A. Bandilla: *Opt. Commun.* **80** (1991) 267

[13] M.O. Scully, W.E. Lamb, Jr.: *Phys. Rev.* **159** (1967) 208

[14] A. Bandilla, H. Voigt: *Opt. Commun.* **43** (1982) 277